Materials Horizons

ROYAL SOCIETY OF CHEMISTRY

COMMUNICATION

View Article Online
View Journal | View Issue

Cite this: *Mater. Horiz.*, 2022, 9, 350

Received 30th June 2021,
Accepted 5th August 2021

DOI: 10.1039/d1mh01019k

rsc.li/materials-horizons

Substituent-dependent absorption and fluorescence properties of perylene bisimide radical anions and dianions†‡

Rebecca Renner,[a] Matthias Stolte,[ab] Julia Heitmüller,[c] Tobias Brixner,[bc] Christoph Lambert[ab] and Frank Würthner[*ab]

Perylene-3,4:9,10-bis(dicarboximides) (PBIs) rank among the most important functional dyes and organic semiconductors, but only recently have their radical anions and dianions attracted interest for a variety of applications. Here, we systematically elucidate the functional properties (redox, absorption, and emission) of five PBI anions and dianions bearing different bay-substituents attached to the chromophore core. Cyclic voltammetry measurements reveal the influence of the substituents ranging from electron-withdrawing cyano to electron-donating phenoxy groups on the oxidation and reduction potentials that relate to the HOMO and LUMO levels ranging from −7.07 eV to −6.05 eV and −5.01 eV to −4.05 eV, respectively. Spectroelectrochemical studies reveal a significant number of intense absorption bands in the NIR-spectral range (750–1400 nm) for the radical anions, whereas the dianionic species are characterized by similar spectra to those for the neutral dyes, however being bathochromically shifted and with increased molar extinction coefficients of approximately 100 000 M^{-1} cm^{-1}. The increase of the transition dipole moment is up to 56% and accompanied by an almost cyanine-like red-shifted (by 300 nm) absorption spectrum for the most electron-poor tetracyanotetrachloro PBI. Whilst the outstanding fluorescence properties of the neutral PBIs are lost for the radical anions, an appreciable near-infrared (NIR) fluorescence with a quantum yield of up to 18% is revealed for the dianions by utilizing a custom-built flow-cell spectroelectrochemistry setup. Time-dependent density functional theory calculations help to assign the absorption bands to the respective electronic transitions.

New concepts

During the last decade our group has made many contributions to the field of perylene bisimide dyes that constitute a most versatile class of absorbers, emitters and redox systems. Furthermore, they are widely utilized as building blocks for aggregates and functional materials. Most recently, new perspectives arose for perylene bisimides in electro- and photocatalysis. In this regard it is surprising that the properties of their radical anions and dianions remained rather unexplored despite their importance for many of these applications. After we were recently able to establish a custom-made setup for the controlled generation of specific redox states in our optical spectrometers, we could characterize not only the absorption but also the emission properties of the reduced species, as described in the current manuscript. We expect that this fundamental study will be most useful for everyone interested in radical anionic and dianionic species of perylene bisimide dyes, *i.e.* researchers interested in photoinduced electron transfer reactions, battery materials, photocatalysis, organic photovoltaics, *etc.*

Introduction

About 100 years ago, perylene-3,4:9,10-bis(dicarboximide) (PBI) dyes firstly attracted attention as vat dyes and later on as industrial pigments.[1–3] When used as vat dyes, the water-insoluble PBI pigment is reduced to the soluble leuco form, corresponding to an anionic species, which can be processed easily in textile or paper dying and other applications. Upon exposure of this reduced species to air the dye is re-oxidized, similar to indigo,[4] giving the coloured fabric.[5] Due to the straightforward adjustability of optical (absorption, emission) and electronic (ionization potential, electron affinity) properties of PBIs by substitution, a large variety of PBI derivatives has been developed in particular during the last decade.[6,7] By this

[a] *Universität Würzburg, Institut für Organische Chemie, Am Hubland, 97074 Würzburg, Germany. E-mail: wuerthner@uni-wuerzburg.de*
[b] *Universität Würzburg, Center for Nanosystems Chemistry (CNC), Theodor-Boveri-Weg, 97074 Würzburg, Germany*
[c] *Universität Würzburg, Institut für Physikalische und Theoretische Chemie, Am Hubland, 97074 Würzburg, Germany*

† Dedicated to Prof. Seth Marder on the occasion of his 60th birthday.

‡ Electronic supplementary information (ESI) available: General and synthetic methods; additional electrochemical and optical measurements as well as additional theoretical calculations. See DOI: 10.1039/d1mh01019k

means, more sophisticated optoelectronic applications of PBIs emerged in n-channel organic field effect transistors (OFETs),[8,9] ion batteries,[10] electrocatalytic reduction of oxygen to hydrogen peroxide,[11] organic light emitting diodes (OLEDs)[12,13] and organic photovoltaics (OPVs).[14,15] These applications, similar to the vat dying process, rely on the electron-deficient character of the PBI core and the formation of comparably stable delocalized radical anions and dianions upon the addition of electrons.[16–18] Likewise, PBIs enjoy great popularity as acceptor components in molecular dyads due to the formation of stable and spectroscopically characteristic anionic species.[19–21] More recently, the use of PBI radical anions and dianions generated by photoexcitation in the presence of triethylamine was further demonstrated as photosensitizers, catalysing the dehalogenation reaction of a broad variety of aryl halides, further revealing the versatile applicability of the robust reduced PBI species.[22,23] Investigations by transient absorption (TA) spectroscopy proved the efficient photoinduced electron transfer from the excited doublet state of the PBI radical anion to electron acceptors.[24,25] This characteristic of PBIs and related rylene bisimides might be further utilized in the development of new photosensitizers as catalysts for reactions, which would otherwise need highly negative potentials. In this regard Xie and coworkers just recently demonstrated the stepwise reduction of a PBI dye under irradiation, used for the injection of an electron into TiO_2 nanoparticles coated with platinum as a co-catalyst, which could be used for the efficient reduction of water into hydrogen.[26]

Chemical reduction of PBIs remains a field to be further explored, as reports are relatively scarce due to the ambient instability of most reduced PBIs. Accordingly, most anions and dianions reported in the literature are generated *in situ* electrochemically or chemically by reduction with sodium dithionite in deoxygenated water, affording stable solutions for months due to the delocalized aromatic character of these PBI dyes.[16,18,27] Unfortunately, these species cannot be easily isolated from solution. The first report of an isolated and completely characterized, albeit zwitterionic radical anion that is stable under ambient conditions shows the feasibility of the generation of isolable PBI radical anions in general.[28] This organic zwitterion can be considered as a PBI radical anion, which is stabilized by a σ-bonded imidazolium cation. Furthermore, it can be reduced or oxidized further by titration with tetrabutylammonium fluoride or nitrosyl tetrafluoroborate, respectively. In the same year, an extremely electron-poor PBI, having chlorine atoms attached in bay-positions as well as cyano groups in *ortho*-positions was isolated and characterized by single crystal X-ray diffraction.[29] Reduction of this molecule with palladium on activated charcoal, hydrogen and sodium hydrogen carbonate gave the PBI dianion disodium salt, which was stable even under ambient conditions for months.[29] In the following years, more examples of ambient stable radical anions and dianions have been reported, using more moderate reducing agents like potassium carbonate in DMF[30,31] or tetraphenylphosphonium iodide.[32]

Usually, characterization of the reduced species remains scarce and only qualitative UV/Vis/NIR absorption spectra of the neutral as well as reduced species are reported, while insights into emission properties are missing. Recently, after Rybtchinski's first observation of fluorescence for the parent core-unsubstituted PBI dianion,[27] we were able to disclose the first example of a fluorescence spectrum for the dianion of a tetraphenoxy-substituted PBI, utilizing a flow-cell setup that enabled the investigation of the emission as well as femtosecond and coherent two-dimensional (2D) electronic spectroscopy measurements.[33] The latter technique indeed points to another major application of PBI dyes as acceptors in donor–acceptor dyads. Here, PBIs are the preferred acceptors due to the characteristic signature of the PBI radical anion bands in the NIR spectral range.[34] However, whilst TA signatures can be easily assigned for those PBIs that have been characterized by spectroelectrochemistry, they are not available for the vast majority of core-substituted PBIs that could be of value for such studies due to the tunability of their redox properties. Because until now, a concise series of PBIs with a systematic variation of their redox properties has been missing, we herein investigate PBIs in the neutral as well as in their radical anionic and dianionic states for a consistent series of five PBI dyes bearing the 2,6-diisopropylphenyl imide (Dipp) substituent and different bay-substituents by electrochemical and spectroelectrochemical measurements. Furthermore, we also investigate the emission properties for the dianions of this series of PBIs. Within our series, the respective first reduction potential varies by about 1 eV and also comprises planar as well as heavily twisted chromophores. Furthermore, (time-dependent) density functional theory ((TD-)DFT) calculations have been performed to systematically assess the origin of the observed molecular properties and spectral features of the differently charged species.

Results and discussion

Molecular design and chemical reduction

Five PBIs have been chosen for the investigation of their molecular properties in their neutral as well as reduced states. Three of them (**PBI–Cl**, **PBI–H**, and **PBI–OPh**) are commonly applied as organic semiconductors[35–38] or fluorescent dye derivatives,[39] whilst the two others complement the series based on a comparably very high reduction potential (**PBI–ClCN**, see ESI‡)[29] and a fixed helical twist (**PBI–Ph**)[40], which seem to be important for the successful application of these PBIs as non-fullerene acceptors in OPV (Fig. 1a).[41,42] For all derivatives, the bulky 2,6-diisopropylphenyl (Dipp) has been chosen as the imide residue to prevent aggregation and ensure a high solubility.

Generally, either chemical reduction, photoinduced electron transfer or electrochemical reduction can be used to obtain the reduced species of PBIs. Advantageous of the former method would be the straightforward measurement of the desired species by a variety of techniques without the need for elaborate

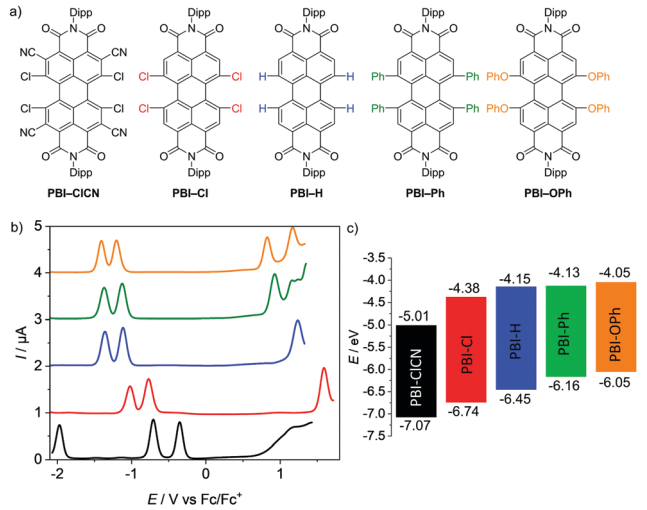

Fig. 1 (a) Molecular structures of the PBIs with bulky 2,6-diisopropylphenyl (Dipp) imide substituents investigated by electrochemical reduction. (b) Square wave voltammograms of **PBI–ClCN** (black), **PBI–Cl** (red), **PBI–H** (blue), **PBI–Ph** (green) and **PBI–OPh** (orange). Measurements were performed using DCM solutions ($c_0 = 2 \times 10^{-4}$ M) at room temperature, using TBAHFP (0.1 M) as electrolyte (scan rate 100 mV s^{-1}, SW amplitude 25 mV, SW frequency 15 Hz). (c) Schematic diagram of the electrical band gaps of the investigated PBIs (energy level of Fc/Fc^+ with respect to the vacuum level = −5.15 eV).[15]

setups due to different measurement geometries and accordingly we first pursued the reduction with KC_8 in THF.[43] As the stoichiometric addition of the reducing agent did not give the desired dianions, an excess of up to four equivalents of the reducing agent was used. The reaction could be monitored by the naked eye, due to prominent changes of the coloured PBI solutions. Upon the addition of 18-crown-6 to the solution, the reaction was significantly accelerated. All the obtained products could be dissolved in 1,2-difluorobenzene for the measurement of UV/Vis/NIR absorption spectra. However even under inert conditions, the oxidation of the generated dianions into the radical anions was observed (Fig. S7, ESI‡). The increased stability of the radical anions compared to the dianions is quite remarkable and has already been observed for other organic radical anions.[43,44] As the stability of the dianions for hours in solution would be necessary for the full characterization of their optical properties, this reduction method did not provide the needed species with sufficient selectivity. Furthermore, the spectra could only be measured in the rather exotic solvent 1,2-difluorobenzene due to an even more pronounced instability in other solvents. As more common solvents like dichloromethane or chloroform are desirable to be more comparable to the literature reported TA spectra, we focused our attention on the electrochemical reduction to spectroscopically characterize the radical anions and dianions of all PBIs.

Cyclic and square wave voltammetry

The redox properties of the PBI series have been investigated by cyclic voltammetry (CV) and square wave (SW) voltammetry under identical experimental conditions in dichloromethane (DCM) using tetrabutylammonium hexafluorophosphate (TBAHFP) as the electrolyte. The SW voltammograms as well as a schematic diagram of the electrical band gaps are depicted in Fig. 1b and c and the half-wave potentials and the calculated HOMO and LUMO potentials are listed in Table 1 (Fig. S4–S6, ESI‡). At least two reversible reduction waves are observed for all five derivatives. Values range from −0.14 V for the first reduction and −0.48 V for the second reduction of the strongest electron acceptor **PBI–ClCN**, which are in line with the reported values for a derivative thereof,[29] to −1.10 V and −1.29 V for the first and second reduction waves, respectively, for the weakest electron acceptor **PBI–OPh**.[45] The other derivatives follow the expected sequence by exhibiting their first reduction wave at −0.77 V for **PBI–Cl**, −1.00 V for **PBI–H** and −1.02 V for **PBI–Ph**, respectively. The potentials of the second reduction wave follow the same trend with values of −1.02 V, −1.22 V and −1.25 V for the latter three PBIs, respectively. Interestingly, the first and second reduction potentials of the planar **PBI–H** and the heavily twisted **PBI–Ph** are very similar, indicating the comparably small influence of a directly attached aryl unit compared to stronger electron withdrawing groups like halogens or electron donating aryloxy groups on the electronic properties of the molecule. Integration of the first and second reduction peaks in the SW spectra proved that the ratio of the electronic quantity of the reduction processes from PBI to $PBI^{\bullet-}$ and $PBI^{\bullet-}$ to PBI^{2-} is one, substantiating the nature of the proposed reduced species. A third reversible reduction wave at −1.73 V could only be observed for **PBI–ClCN**, accentuating the electron deficiency of this derivative due to the additional cyano groups in the *ortho*-position. The effect of the substituents on the redox potentials is even more pronounced for their respective

Table 1 Summary of the redox properties of the investigated PBIs. Half-wave potentials were determined by CV or SWV measurements in DCM (0.1 M TBAHFP) *vs.* Fc/Fc^+ at room temperature

	$E_{1/2}^{Red1}$ [V]	$E_{1/2}^{Red2}$ [V]	$E_{1/2}^{Red3}$ [V]	$E_{1/2}^{Ox1}$ [V]	$E_{1/2}^{Ox2}$ [V]	E_{HOMO} [b] [eV]	E_{LUMO} [b] [eV]	ΔE_{gap}^{CV} [eV]	ΔE_{gap}^{Opt} [eV]
PBI–ClCN	−0.14	−0.48	−1.73	—[a]	—[a]	−7.07[c]	−5.01	2.06	2.13[d]
PBI–Cl	−0.77	−1.02	—[a]	+1.59	—[a]	−6.74	−4.38	2.36	2.21
PBI–H	−1.00	−1.22	—[a]	+1.30	—[a]	−6.45	−4.15	2.30	2.26
PBI–Ph	−1.02	−1.25	—[a]	+1.01	+1.19	−6.16	−4.13	2.03	1.82
PBI–OPh	−1.10	−1.29	—[a]	+0.90	+1.21	−6.05	−4.05	2.00	1.99

[a] Not observed. [b] Calculated according to the known literature procedure using the experimentally determined redox potentials ($E_{HOMO} = -[E_{1/2}^{Ox1} + 5.15\ eV]$ and $E_{LUMO} = -[E_{1/2}^{Red1} + 5.15\ eV]$) and the energy level of Fc/Fc^+ with respect to the vacuum level (−5.15 eV).[15] [c] Calculated according to $E_{HOMO} = E_{LUMO} - E(\lambda_{max})$. [d] Optical band gap higher than electronic band gap probably due to distortion of the band shape due to the overlap of different transitions. Elaborate calculations taking correction factors into account can be found in Table S1 and Table S2 in the ESI.

oxidation processes.[45] Due to the highly electron-deficient character of **PBI–ClCN**, no oxidation could be observed within the available potential range of the used electrolyte system, whereas one oxidation process is observed at +1.59 V and +1.30 V for **PBI–Cl** and **PBI–H**, respectively. Due to the shift of the oxidation waves to lower potentials, two oxidation processes are observable for the other two PBIs at +1.01 V and +1.19 V for **PBI–Ph** and +0.90 V and +1.21 V for **PBI–OPh**. The values are summarized in Table 1. The HOMO and LUMO energy levels have been calculated from the half-wave potentials of the first oxidation and reduction processes, which were obtained by the CV measurements with the energy level of the ferrocene/ferrocenium redox couple set to −5.15 eV *vs.* vacuum.[15] They cover a broad range of almost 1 eV within this series between −7.07 eV and −6.05 eV for the HOMOs and −5.01 eV and −4.05 eV for the LUMOs for **PBI–ClCN** and **PBI–OPh** (Fig. 1c), respectively. Notably, **PBI–ClCN** ranks according to this analysis among the most electron-deficient π-cores, comparable to tetracyanoquinodimethane (TCNQ).[46,47]

UV/Vis/NIR absorption properties in neutral and reduced states

The UV/Vis/NIR absorption spectra of the neutral, radical anionic and dianionic PBIs in DCM could be obtained by electrochemical reduction *in situ* with a custom built spectro-electrochemical cell and are depicted in Fig. 2 and the derived data are collected in Table 2 (for details see the ESI‡ and Fig. S8–S18, Table S3). The optical band gap calculated with the help of the absorption spectra of the neutral species and extrapolation by a linear curve (Tauc's plot)[48] is in all cases, except **PBI–ClCN**, lower in energy than the electrical band gap, which is expected since the threshold for the absorption of photons is smaller than the threshold for the creation of an electron–hole pair.[49]

In accordance with earlier results for these and related PBIs,[1] the unsubstituted planar **PBI–H** exhibits an intense absorption band of the S_0-S_1 transition with vibronic progression with an absorption maximum (λ_{max}) at 527 nm and a high molar extinction coefficient (ε_{max}) of 93 700 M^{-1} cm^{-1} in DCM. Upon substitution in the bay-position, as is the case for all other derivatives within this series, the spectra become more broadened and show a decrease in ε_{max} and the vibronic progression of the S_0–S_1 transition is less clearly visible. Furthermore, the S_0–S_2 transition, which is symmetry forbidden for the planar chromophore,[50] becomes allowed and can be observed as a second absorption maximum at about 440 nm. This effect is most pronounced for **PBI–Ph**, which contains the most twisted chromophore.[40] The attachment of electron withdrawing halogen atoms in the bay-position does not exhibit a large influence on the absolute position of the absorption maximum (**PBI–Cl** 522 nm; **PBI–ClCN** 531 nm), whereas the more electron donating groups like tetraaryl (**PBI–Ph** 609 nm) or tetraaryloxy (**PBI–OPh** 576 nm) afford a significant redshift, reflecting electronic interactions, *i.e.*, electron donation from the bay-substituents to the PBI core.[51]

Under the influence of an electrochemical potential between −0.1 and −1.2 V, significant spectral changes occur for all PBI

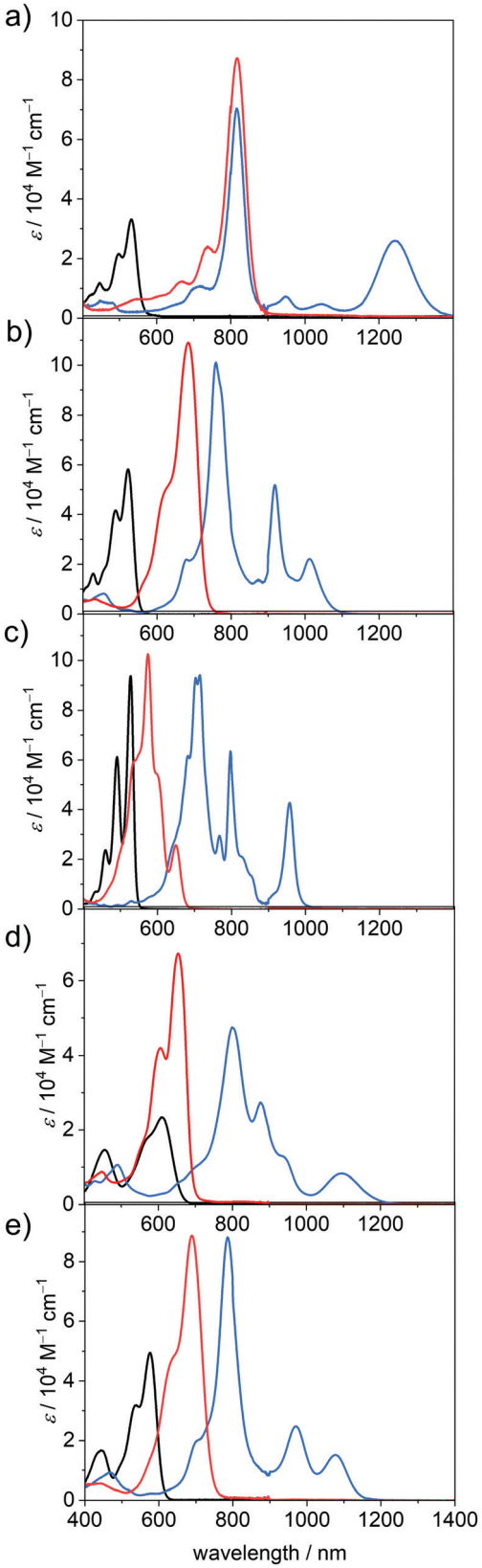

Fig. 2 UV/Vis/NIR absorption spectra of the neutral (black), radical anionic (blue) and dianionic (red) PBI species of (a) **PBI–ClCN**, (b) **PBI–Cl**, (c) **PBI–H**, (d) **PBI–Ph**, and (e) **PBI–OPh** measured in DCM (c_0 = 4 × 10^{-4} M) at room temperature using TBAHFP (0.1 M) as electrolyte.

Table 2 Summary of the absorption and emission properties of the investigated PBIs and their electrochemically generated dianions measured in DCM (0.1 M TBAHFP) at room temperature

	λ_{max} [nm]	ε_{max} [M^{-1} cm^{-1}]	μ_{eg} [D]	λ_{em}[a] [nm]	$\Delta\tilde{\nu}_{Stokes}$ [cm^{-1}]	Φ_f[b] [%]	τ_F[c] [ns]
PBI–ClCN	531	33 900	—[d]	575	1510	0.1	0.15, 2.10
PBI–ClCN^{2-}	817	87 200	—[d]	—[e]	—[e]	—[e]	—[e]
PBI–Cl	522	58 200	8.7	549	940	57	5.06
PBI–Cl^{2-}	684	109 100	12.6	722	770	3	2.04
PBI–H	527	93 700	8.8	534	210	99	3.72
PBI–H^{2-}	574	102 600	3.5	662	300	18	5.92
PBI–Ph	609	23 400	6.4	677	1650	46	10.87
PBI–Ph^{2-}	653	67 300	10.0	676	520	15	4.36
PBI–OPh	576	49 600	8.7	608	915	96	6.01
PBI–OPh^{2-}	689	88 700	12.4	738	960	17	3.93

[a] Fluorescence spectra of PBI^{2-} have been measured in front-face geometry (22.5°) and all spectra are corrected against the photomultiplier sensitivity and the lamp intensity. [b] Fluorescence quantum yields of the neutral PBIs were determined using the dilution method (OD < 0.05) and *N*,*N*′-bis(2,6-diisopropylphenyl)-perylene-3,4:9,10-bis(dicarboximide) (Φ_F = 1.00 in $CHCl_3$) or *N*,*N*′-bis(2,6-diisopropylphenyl)- 1,6,7,12-tetraphenoxy-perylene-3,4:9,10-bis(dicarboximide) (for **PBI–OPh**, Φ_F = 0.96 in $CHCl_3$)[39] as reference. Fluorescence quantum yields of PBI^{2-} were determined relative to PBI by excitation at 385 nm (**PBI–Cl**), 415 nm (**PBI–H**), 490 nm (**PBI–Ph**) and 398 nm (**PBI–OPh**). [c] Fluorescence lifetimes were determined with EPL picosecond pulsed diode lasers for time-correlated single photon counting (λ_{ex} = 530 nm (**PBI–ClCN**), λ_{ex} = 550 nm (**PBI–Cl**, **PBI–H**, **PBI–OPh**), λ_{ex} = 560 nm (**PBI–Ph**), λ_{ex} = 725 nm (**PBI–Cl^{2-}**), λ_{ex} = 662 nm (**PBI–H^{2-}**), λ_{ex} = 725 nm (**PBI–Cl^{2-}**), λ_{ex} = 677 nm (**PBI–Ph^{2-}**), λ_{ex} = 735 nm (**PBI–OPh^{2-}**)). [d] Significant overestimation due to multiple transitions present in the S_0–S_1 absorption band. [e] Not observed.

dyes in DCM. All radical anions exhibit multiple characteristic spectral features in the UV/Vis/NIR region, each with a prominent and broad absorption band at 957 nm or above (**PBI–H**), which is commonly assigned to the D_0-D_1 transition (*vide infra*).[52] In the case of **PBI–ClCN** this NIR transition appears at 1243 nm, followed by **PBI–Ph** (1097 nm), **PBI–OPh** (1076 nm) and **PBI–Cl** (1011 nm) (Fig. 2). The absorption spectra in the UV/Vis/NIR region of all five radical anions exhibit at least three clearly distinguishable transitions. The most prominent absorption bands are also bathochromically shifted with respect to those of the neutral PBIs and are found for all derivatives between 715 nm for the unsubstituted **PBI–H** and 817 nm for **PBI–ClCN**. Whereas the electron withdrawing groups exert only a minor influence on the wavelength of the lowest energy absorption band in the neutral state, they affect those of all absorption bands in the radical anionic state in a similarly pronounced way as the electron donating substituents. Furthermore, different from **PBI–H** with an almost unchanged ε_{max} value of 94 100 M^{-1} cm^{-1} upon reduction to the radical anion, a significant increase between 174% (**PBI–Cl**, 101 100 M^{-1} cm^{-1}) up to 212% (**PBI–ClCN**, 70 300 M^{-1} cm^{-1}) in ε_{max} is found for the main absorption band of all the bay-substituted derivatives. Additionally, at least one further transition can be observed between the absorption maximum for the most intense band and the lowest energy absorption band of the radical anions. For the unsubstituted derivative **PBI–H**, even more distinguishable absorption features than for the other PBIs are found, which originate from the more rigid and planar π-scaffold, similar to the neutral species. These intense and characteristic absorption bands make the here investigated PBI derivatives particularly valuable for the investigation of photoinduced electron transfer processes in molecular dyads as well as solid state materials.[52]

Upon further reduction at a bias between −0.4 and −1.3 V, the absorption spectra of all PBI dianions simplify to one prominent absorption band that is located between 650 and 900 nm. This hypsochromic shift with respect to the NIR bands of the radical anion species is accompanied by an additional increase in band intensity. Thus, the values for ε_{max} increase further for all the derivatives to more than 100 000 M^{-1} cm^{-1} in the case of **PBI–Cl** (684 nm) and **PBI–H** (574 nm) and to more than twice the intensity of the respective neutral species in the cases of **PBI–Ph** (67 300 M^{-1} cm^{-1} at 653 nm) and **PBI–ClCN** (87 200 M^{-1} cm^{-1} at 817 nm). Surprisingly, only the dianion of the parent **PBI–H** displays an optical spectrum of rather different shape with a transition at 649 nm of lower intensity (25 600 M^{-1} cm^{-1}) followed by a strong absorbing and structured absorption spectrum at about 574 nm. The increase in tinctorial strength for these PBI dianions is indeed remarkable. Integration of the respective isolated longest wavelength S_0–S_1 absorption bands of the neutral and the dianionic species shows again an increase in the transition dipole moments μ_{eg} from 8.7 to 12.6 D (**PBI–Cl**), 6.4 to 10.0 D (**PBI–Ph**) and 8.7 to 12.4 D (**PBI–OPh**) for all derivatives except **PBI–H**, where it decreases from 8.8 to 3.5 D (Table 2). Some of these values might be overestimated due to the presence of multiple transitions in the respective S_0-S_1 absorption band (*vide infra*).

Fluorescence properties in the neutral and dianionic states

The fluorescence spectra, fluorescence quantum yields (Φ_f) and fluorescence lifetimes (τ_F) of the five neutral PBIs and four dianionic PBIs could be obtained within an SEC flow-cell setup (Fig. 3, Table 2 and Fig. S8b, S20–S22, ESI‡). As expected, all the radical anions showed no emission. The Φ_f of the dianions were determined relative to the respective neutral species within one SEC run, while the fluorescence decay curves were recorded by time-correlated single-photon counting (TCSPC) in front-face geometry (22.5°). All emission spectra of the neutral and dianionic PBIs show mirror-like shape with respect to their corresponding absorption spectra, with the exception of **PBI–Ph^{2-}**, which exhibits an unexpected narrow fluorescence band with a well-defined vibronic progression. All the bay-

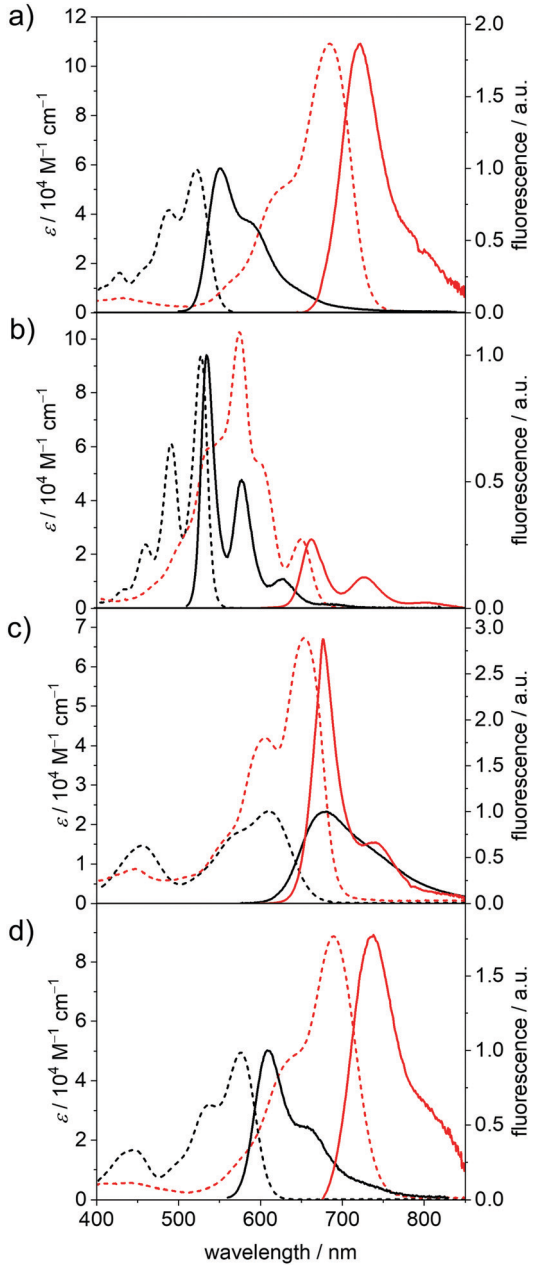

Fig. 3 UV/Vis/NIR absorption spectra (dashed lines) as well as the fluorescence spectra (solid lines) of the neutral (black) and dianionic (red) (a) **PBI–Cl**, (b) **PBI–H**, (c) **PBI–Ph** and (d) **PBI–OPh** measured in DCM (c_0 = 4 × 10^{-4} M for absorption, c_0 = 1 × 10^{-5} M for fluorescence of PBI and c_0 = 1 × 10^{-4} M for fluorescence of PBI^{2-}) at room temperature using TBAHFP (0.1 M) as electrolyte.

substituted PBIs show almost equal (**PBI–OPh**$^{2-}$) or even decreased Stokes shifts ($\Delta\tilde{\nu}_{Stokes}$) in their dianionic states, while the unsubstituted **PBI–H** exhibited a slight increase from 210 cm^{-1} (PBI) to 300 cm^{-1} (PBI^{2-}), which is still smaller than the $\Delta\tilde{\nu}_{Stokes}$ of the other derivatives due to the more rigid framework and lack of substituents. The same holds true for τ_F, which is increased again only for **PBI–H** from 3.72 ns (PBI) to 5.92 ns (PBI^{2-}), while it is decreased in all other derivatives upon reduction.

The Φ_f of all dianions are significantly reduced as expected for the emission due to the decreased band gap[53] but are still appreciably high with 18% at 662 nm (**PBI–H**$^{2-}$) and 17% at 738 nm (**PBI–OPh**$^{2-}$) compared to, *e.g.*, higher rylene dyes emitting in the region between 650 and 950 nm.[54–56] For **PBI–Cl**$^{2-}$ an emission maximum at 722 nm, with reduced $\Delta\tilde{\nu}_{Stokes}$ of 770 cm^{-1} and the most pronounced decrease of the quantum yield within this series is noted from 57% (PBI) to 3% (PBI^{2-}). **PBI–Ph** exhibits a large $\Delta\tilde{\nu}_{Stokes}$ of 1650 cm^{-1} affording λ_{em} of 677 nm. This indicates the participation of the core-substituents in the lowest excited state upon photoexcitation and the following structural relaxation.[20] Interestingly, the Φ_f of the arylated dye does not decrease as significantly upon reduction as the other derivatives, from 46% of the neutral **PBI–Ph** to 15% for **PBI–Ph**$^{2-}$. Together with the structured fluorescence spectrum such high quantum yield corroborates the rigidification effect impaired by the four phenyl units that are interlocked based on the crystallographic evidence from the related chromophores.[57] The neutral **PBI–ClCN** exhibits only very weak fluorescence upon excitation at 490 nm, with a λ_{em} at 575 nm and a Φ_f of merely 0.1%. Because this is much lower than the reported quantum yield of 11% of the neutral congener with electron-withdrawing fluoroalkyl chains in the imide position we attribute the fluorescence quenching to a photoinduced electron transfer from the Dipp substituent into the highly electron-deficient core.[58] Similar processes have been reported for the more electron-rich imide substituents to the parent electron-poor PBI.[20,59]

The decrease of Φ_f upon reduction for all the derivatives can be ascribed to an increase of the rate of non-radiative decay processes, as expected due to the smaller band gap for the dianionic state.[60] The trend observed in τ_F corresponds to the trend obtained for the natural lifetimes τ_0 by analysis according to the Strickler–Berg relationship.[61] For **PBI–H**, τ_0 is slightly increased in the dianion (3.64 ns to 3.75 ns), while for the other three derivatives **PBI–Cl** (5.14 ns to 4.50 ns), **PBI–Ph** (17.5 ns to 5.08 ns) and **PBI–OPh** (6.89 ns to 5.22 ns) τ_0 is decreased in the measured reduced state of the molecules due to the increase of the transition dipole moment and oscillator strength. The radiative decay rates k_r obtained by this analysis nevertheless decrease in all the derivatives upon reduction, while the non-radiative decay rates k_{nr} are increased, confirming the experimental results of the decreasing quantum yields in the PBI dianions.

Theoretical investigations

In order to further elucidate the trends observed by optical spectroscopy upon electrochemical reduction, (time-dependent) density functional theory ((TD-)DFT) calculations were performed. For simplicity, the Dipp imide residues were replaced by methyl groups, as their impact on the molecular properties of the chromophore is negligible.[62]

The geometry-optimized structures of all derivatives with the exception of **PBI–H** exhibit a large twist of the two naphthalene subunits between 31.0° (**PBI–OPh**) and 39.5° (**PBI–ClCN**). This results in a distortion of the PBI π-MO system. In all derivatives

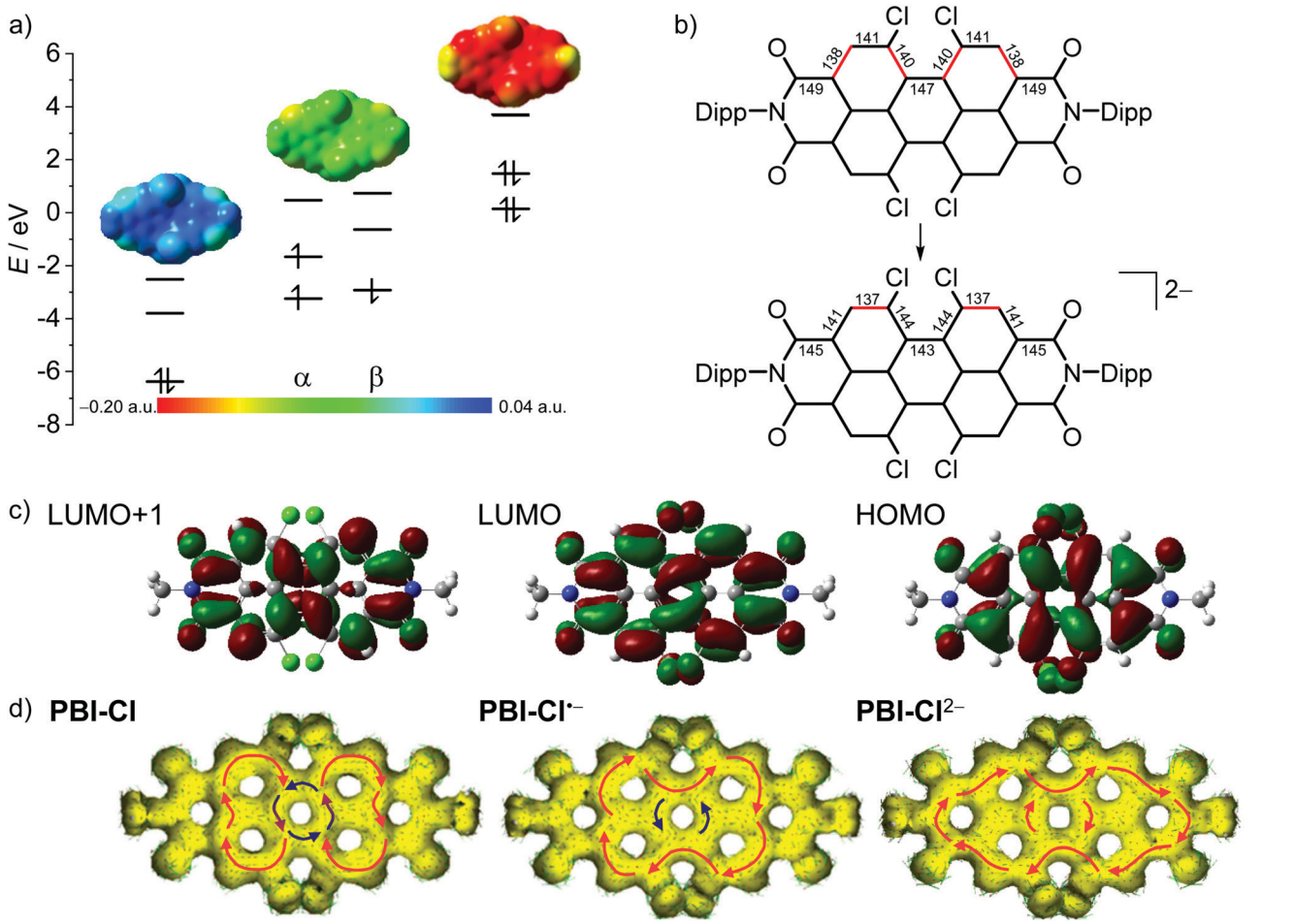

Fig. 4 (a) The HOMO, LUMO and LUMO+1 levels as obtained from DFT calculations of **PBI–Cl** (left), the corresponding α- and β-spin MO levels of **PBI–Cl**$^{\bullet-}$ (middle) and HOMO−1, HOMO and LUMO levels of **PBI–Cl**$^{2-}$ (right), as well as the electrostatic potential maps of the respective derivative (top, isovalue 0.020 a.u.). (b) Calculated bond length for perylene carbon–carbon bonds in neutral and dianionic states in pm (for details, see Table S4, ESI‡). Bonds drawn in red indicate a high double-bond character. (c) The HOMO, LUMO and LUMO+1 (right to left) of **PBI–Cl**. The corresponding orbitals of **PBI–Cl**$^{\bullet-}$ and **PBI–Cl**$^{2-}$ are visually indistinguishable. Orbitals and electrostatic potential maps were calculated using DFT (B3LYP/6-31g(d)). (d) Calculated AICD isosurface plots of **PBI–Cl**, **PBI–Cl**$^{\bullet-}$ and **PBI–Cl**$^{2-}$. Clockwise ring current is depicted with red arrows and counterclockwise ring current with blue arrows (isosurface value 0.025).

the LUMO of the neutral PBI, the SOMO of the radical anion (PBI$^{\bullet-}$) and the HOMO of the dianion (PBI^{2-}) are visually indistinguishable and thus in Fig. 4 (Fig. S24 and 25, ESI‡) only the MOs of the neutral PBI are shown.

As depicted in Fig. 4b for the tetrachlorinated **PBI–Cl** there are significant changes in bond length upon reduction from the neutral to the dianionic state. Whilst the changes in bond length are comparably minor for the inner bonds of the perylene (<3 pm), the conjugated outer perimeter experiences a significant alteration where bonds either get shorter by up to 3.8 pm from 148.5 pm to 144.7 pm or longer by up to 3.4 pm from 138.0 pm to 141.4 pm. This change in bond length relates to a reversal of single *versus* double bond character, which is in accordance with the bonding character between the involved atoms in the LUMO (Fig. 4c). As a consequence, the PBI skeleton of **PBI–Cl** (and likewise the other derivatives) is contracted by about 66 pm along the long molecular axis upon twofold reduction and expanded by about 57 pm along the short axis. It is interesting to relate these bond length alterations to the carbon–carbon bond stretching vibration that occurs upon photoexcitation of PBI into the S_1 state, *i.e.*, promotion of an electron from the HOMO into the LUMO, and that causes the characteristic vibronic progression in the absorption and fluorescence bands of PBIs. The most striking change of bond length concerns the bonds connecting the two naphthalene subunits, *e.g.*, in the tetrachlorinated **PBI–Cl** from 146.8 pm for the neutral PBI *via* 144.8 pm for the radical anion to 143.1 pm in the dianion (Table S4, ESI‡). This decreased bond length in the dianion for the central connections between the naphthalene subunits as well as the bond length alterations for the peripheral C–C carbon chain is in accordance with calculations by Iron, Rybtchinski and co-workers for the unsubstituted PBI[16,27] and our experimental results by single-crystal X-ray analysis for a derivative of **PBI–ClCN**.[29] This corroborates a stiffening of the π-scaffold for the central ring and planarization of the PBI core with a reduction of the twist angle from

35.4° to 31° in **PBI–Cl** due to the additional electron density in the system (Table S4, ESI‡).

The transitions to the excited states obtained by TD-DFT calculations are in good accordance with the experimental results concerning the number and intensities of the observed transitions (Fig. S23, Table S5–S19, ESI‡). While the calculated transition energies agree reasonably well with the neutral PBIs, *e.g.*, **PBI–H** with 488 and 527 nm for the calculated and experimental spectra, respectively, they deviate in some examples of the radical anions and dianions quite severely. Nevertheless, the bathochromic shift of the radical anion spectra visible in all derivatives, as well as the subsequent hypsochromic shift of the most prominent transitions of the dianions is substantiated by the theoretical results. The calculated energies for the allowed optical transitions could be correlated to the respective experimental values well enough by shifting the whole spectrum, so that the transitions with the highest oscillator strength exhibit the same energy as the absorption maximum in the experimental absorption spectrum, allowing for an assignment of the individual absorption bands (Fig. S23, ESI‡) with which some further conclusions could be made (*vide infra*).

According to the calculations, for the neutral state of the most electron-deficient **PBI–ClCN**, two transitions are quite close in energy around 570 nm and thus no clear separation thereof can be observed in the experimental spectra (Table S5, ESI‡). In the other three bay-substituted derivatives, the bands of the experimental spectra could be assigned to the S_0–S_1 transition as well as the S_0–S_2 transition at slightly higher energies. In the planar unsubstituted **PBI–H**, only the S_0–S_1 transition exhibits a noteworthy oscillator strength, corresponding to former reports and the symmetry forbiddance of the S_0–S_2 transition.[63] Due to the spin-separated energy levels in the radical anionic state, the assignment of the transitions is more complex. In the bay-chlorinated PBIs **PBI–ClCN** and **PBI–Cl** the SOMO–LUMO transition corresponds to the lowest-energy transition in the NIR region and thus can be assigned to D_0–D_1 transition. The same holds true for **PBI–OPh**. In the unsubstituted **PBI–H**, this transition causes the absorption band at 649 nm in the calculated spectrum, while the most bathochromically shifted absorption band corresponds to a transition of the electron from the highest occupied β-spin orbital to the lowest unoccupied β-spin orbital. In the tetraphenyl derivative **PBI–Ph**, the SOMO–LUMO transition corresponds to the absorption maximum at 679 nm, while for the lowest-energy absorption band a similar transition of the electron in the β-MO as in **PBI–H** is found. The predictions for optically allowed transitions of PBI radical anions are probably less accurate than the predictions for the neutral and dianionic species due to the radical nature of the PBIs and the neglect of solvent effects.[16]

In the calculated transitions of the dianions, the HOMO–LUMO transition thereof corresponds to the lowest-energy transition in all derivatives except for **PBI–Cl** and **PBI–OPh**. For these two derivatives, the lowest-energy transition is not well described by the simple HOMO–LUMO transition but rather by a HOMO–LUMO+1 transition, which suggests that the excitation energy is actually not equal to the HOMO–LUMO orbital energy difference. Thus, even though the calculations are of good assistance in the interpretation of the experimental spectra, the reality might be more complex. In accordance with the experimental UV/Vis/NIR spectrum of **PBI–H^{2-}**, the calculations predict a significantly smaller oscillator strength of 0.0938 for the S_0-S_1 transition than for the S_0-S_2 transition with 0.8905 (see Fig. 2c and Table S13, ESI‡). The intensity of the absorption bands relates to the oscillator strength or the transition dipole moment.

Unfortunately, the experimental determination of the transition dipole moments (μ_{eg}) of some derivatives, especially in their reduced states, is not straightforward for this series of dyes due to a significant overlap of different transitions, thus overestimating the values significantly (*vide supra*). However, the values for μ_{eg} of neutral **PBI–Cl**, **PBI–H**, **PBI–Ph** and **PBI–OPh** could be determined by integration of the absorption band corresponding to the S_0–S_1 transition of the experimental spectra to be 8.7 D, 8.8 D, 6.4 D and 8.7 D, which fits reasonably well with the values obtained from TD-DFT calculations of 7.6 D, 8.8 D, 6.6 D and 8.1 D, respectively (Table S20, ESI‡). Theoretical determination of μ_{eg} from TD-DFT calculations for all species shows a decrease of the transition dipole moment for the lowest energy transition upon the first reduction of the PBIs with the exception of the directly arylated **PBI–Ph**, where μ_{eg} of the radical anion is increased compared to the neutral PBI. Upon further reduction to the dianion, a further increase of μ_{eg} is noted for all PBI dyes with values reaching above 9.0 D for most derivatives. Similar to the previous results (*vide supra*), the calculations predict μ_{eg} of all five neutral PBIs as well as their dianionic states reasonably well (Table S20, ESI‡).

The differences in oscillator strength of the first two transitions of **PBI–H^{2-}** compared to the bay-substituted PBIs can be rationalized by investigation of the transition density (Fig. S27, ESI‡). It can be seen that the transition density of the S_0–S_1 transition of **PBI–H^{2-}** is polarized along the short molecular axis and resembles the transition densities of the S_0–S_2 transitions of the four substituted PBI dianions. In contrast, the S_0–S_2 transition density of **PBI–H^{2-}**, which is polarized along the long molecular axis (N,N') exhibits a high oscillator strength in the absorption spectrum, which is comparable to the S_0–S_1 transitions of the substituted PBI dianions; thus the two differently polarized transitions are interchanged in the planar PBI dianion compared to the bay-substituted contorted systems.[64]

To further explore the aromaticity of the different reduced species, anisotropy of the induced current-density (AICD) calculations was performed for **PBI–Cl** and **PBI–H** as well as their respective reduced species.[65,66] In both the neutral molecules, clockwise diamagnetic ring currents can be observed that are localized in the two naphthalene subunits, suggesting a Clar-type localization of aromaticity, while the central PBI ring exhibits a counterclockwise paramagnetic ring current, indicating anti-aromaticity (Fig. 4d, Fig. S28, ESI‡). Upon reduction,

the clockwise ring current expands over the whole PBI core along the outer perimeter and the counterclockwise current in the centre vanishes. This reorganization of the π-electron delocalization has been elucidated before in a theoretical study by Iron and co-workers to explain the high stability of PBI dianions in water due to their increased aromatic character.[16] These results from the AICD calculations match quite well to our earlier observations, *i.e.*, the contraction of the bonds connecting the two naphthalene subunits due to increased conjugation and the increase of the absorption coefficients and bathochromic shifts of the absorption bands observed for PBI dianions.

Conclusion

In this article, the optical properties for a series of five perylene bisimide dyes bearing 2,6-diisopropylphenyl groups in the imide position but different bay-substituents on the π-core have been investigated upon their reduction into radical anionic and dianionic states in custom-built spectroelectrochemical cells for UV/Vis/NIR absorption and emission studies. Their first reduction potentials range almost over 1 V from −0.14 V for the most electron-deficient **PBI–ClCN** to −1.10 V for the most electron-rich **PBI–OPh**. Significant bathochromic shifts of all the absorption spectra upon the first reduction with the most red-shifted maximum at 1243 nm (**PBI–ClCN**) were observed. Upon further reduction, the absorption maxima shift again back hypsochromically compared to the radical anionic spectra. The molar extinction coefficients ε_{max} increase in all derivatives upon reduction to approximately 100 000 M^{-1} cm^{-1}, with absorption maxima between 649 nm (**PBI–H**) and 817 nm (**PBI–ClCN**) for the dianions. While fluorescence data of neutral PBI dyes are abundantly reported, we could study and quantify the fluorescence properties (Φ_f, τ_F, $\Delta\tilde{\nu}_{Stokes}$) of the dianions of the whole series in a custom-built flow-cell setup. While the fluorescence quantum yield was reduced for all PBI dianions, due to an increased influence of non-radiative decay pathways, values of up to 18% (662 nm) and 17% (738 nm) were retained for **PBI–H** and **PBI–OPh**, respectively. DFT and TD-DFT calculations assist in the elucidation of the origin of the experimentally observed absorption bands as well as structural changes of all PBIs and their reduced species. They showed a localization of the MOs on the perylene core rather than on the substituents for the relevant energetic states. Furthermore, the experimental spectra could be brought into line with the calculated absorption spectra. Overall, based on our comprehensive library of five PBIs, electronic and optical properties of their radical anions and their dianions could be characterized in a systematic manner. This information should be of great value for the analysis of PBI-bearing molecular dyads and PBI-based solid-state materials by transient absorption spectroscopy and for the utilization of these dyes as sensitizers for photocatalysis.

Author contributions

Rebecca Renner: investigation, methodology, and visualization. Matthias Stolte: methodology, investigation, and writing. Julia Heitmüller: methodology, writing. Tobias Brixner: writing, supervision, and funding acquisition. Christoph Lambert: writing. Frank Würthner: conceptualization, writing, supervision, and funding acquisition.

Conflicts of interest

There are no conflicts to declare.

Acknowledgements

We would like to thank Dr David Bialas for his assistance with DFT and TD-DFT calculations. We are grateful for the financial support from the Deutsche Forschungsgemeinschaft (Grant Wu 317/20-2).

Notes and references

1 C. Huang, S. Barlow and S. R. Marder, *J. Org. Chem.*, 2011, **76**, 2386–2407.
2 K. Hunger and W. Herbst, *Pigments, Organic in Ullmann's Encyclopedia of Industrial Chemistry*, Wiley-VCH, Weinheim, 2000.
3 W. Herbst and K. Hunger, *Industrial Organic Pigments: Production, Properties, Applications*, Wiley-VCH, Weinheim, 3rd edn, 2004.
4 E. Steingruber, *Indigo and Indigo Colorants in Ullmann's Encyclopedia of Industrial Chemistry*, Wiley-VCH, Weinheim, 2004.
5 M. Greene, *High Performance Pigments*, Wiley-VCH, Weinheim, 2009, ch. 16.
6 A. Nowak-Król and F. Würthner, *Org. Chem. Front.*, 2019, **6**, 1272–1318.
7 F. Würthner, C. R. Saha-Möller, B. Fimmel, S. Ogi, P. Leowanawat and D. Schmidt, *Chem. Rev.*, 2016, **116**, 962–1052.
8 R. Schmidt, J. H. Oh, Y.-S. Sun, M. Deppisch, A.-M. Krause, K. Radacki, H. Braunschweig, M. Könemann, P. Erk, Z. Bao and F. Würthner, *J. Am. Chem. Soc.*, 2009, **131**, 6215–6228.
9 B. A. Jones, A. Facchetti, M. R. Wasielewski and T. J. Marks, *J. Am. Chem. Soc.*, 2007, **129**, 15259–15278.
10 H.-G. Wang, S. Yuan, D.-I. Ma, X.-I. Huang, F.-I. Meng and X.-B. Zhang, *Adv. Energy Mater.*, 2014, **4**, 1301651.
11 M. Warczak, M. Gryszel, M. Jakesova, V. Đerek and E. D. Głowacki, *Chem. Commun.*, 2018, **54**, 1960–1963.
12 S. V. Dayneko, M. Rahmati, M. Pahlevani and G. C. Welch, *J. Mater. Chem. C*, 2020, **8**, 2314–2319.
13 G. Li, Y. Zhao, J. Li, J. Cao, J. Zhu, X. W. Sun and Q. Zhang, *J. Org. Chem.*, 2015, **80**, 196–203.
14 X. Zhan, Z.-A. Tan, B. Domercq, Z. An, X. Zhang, S. Barlow, Y. Li, D. Zhu, B. Kippelen and S. R. Marder, *J. Am. Chem. Soc.*, 2007, **129**, 7246–7247.

15 A. Nowak-Król, K. Shoyama, M. Stolte and F. Würthner, *Chem. Commun.*, 2018, **54**, 13763–13772.
16 M. A. Iron, R. Cohen and B. Rybtchinski, *J. Phys. Chem.*, 2011, **115**, 2047–2056.
17 V. V. Roznyatovskiy, D. M. Gradner, S. W. Eaton and M. R. Wasielewski, *Org. Lett.*, 2014, **16**, 696–699.
18 R. O. Marcon and S. Brochsztain, *Langmuir*, 2007, **23**, 11972–11976.
19 B. Rybtchinski, L. E. Sinks and M. R. Wasielewski, *J. Am. Chem. Soc.*, 2004, **126**, 12268–12269.
20 W. Kim, T. Kim, S. Kang, Y. Hong, F. Würthner and D. Kim, *Angew. Chem., Int. Ed.*, 2020, **132**, 8571–8578.
21 M. S. Rodríguez-Morgande, T. Torres, C. Atienza-Castellanos and D. M. Guldi, *J. Am. Chem. Soc.*, 2006, **128**, 15145–15154.
22 I. Ghosh, T. Ghosh, J. I. Bardagi and B. König, *Science*, 2014, **346**, 725–728.
23 H.-X. Gong, Z. Cao, M.-H. Li, S.-H. Liao and M.-J. Lin, *Org. Chem. Front.*, 2018, **5**, 2296–2302.
24 C. J. Zeman, S. Kim, F. Zhang and K. S. Schanze, *J. Am. Chem. Soc.*, 2020, **142**, 2204–2207.
25 C. Rosso, G. Filippini and M. Prato, *Eur. J. Org. Chem.*, 2021, 1193–1200.
26 Y. Xu, J. Zheng, J. O. Lindner, X. Wen, N. Jiang, Z. Hu, L. Liu, F. Huang, F. Würthner and Z. Xie, *Angew. Chem., Int. Ed.*, 2020, **59**, 10363–10367.
27 E. Shirman, A. Ustinov, N. Ben-Shitrit, H. Weissman, M. A. Iron, R. Cohen and B. Rybtchinski, *J. Phys. Chem. B*, 2008, **112**, 8855–8858.
28 D. Schmidt, D. Bialas and F. Würthner, *Angew. Chem., Int. Ed.*, 2015, **54**, 3611–3614.
29 S. Seifert, D. Schmidt and F. Würthner, *Chem. Sci.*, 2015, **6**, 1663–1667.
30 Q. Li, H. Guo, X. Yang, S. Zhang and H. Zhang, *Tetrahedron*, 2017, **73**, 6632–6636.
31 E. He, J. Wang, H. Liu, Z. He, H. Zhao, W. Bao, R. Zhang and H. Zhang, *J. Mater. Sci.*, 2016, **51**, 9229–9238.
32 Y. Kumar, S. Kumar, D. Bansal and P. Mukhopadhyay, *Org. Lett.*, 2019, **21**, 2185–2188.
33 J. Heitmüller, K. Eckstein, R. Renner, M. Stolte, T. Hertel, F. Würthner and T. Brixner, *Spectrochim. Acta, Part A*, 2021, **253**, 119567.
34 P. E. Hartnett, C. M. Mauck, M. A. Harris, R. M. Young, Y.-L. Wu, T. J. Marks and M. R. Wasielewski, *J. Am. Chem. Soc.*, 2017, **139**, 749–756.
35 L. H. Slooff, E. E. Bende, A. R. Burgers, T. Budel, M. Pravettoni, R. P. Kenny, E. D. Dunlop and A. Büchtemann, *Phys. Status Solidi RRL*, 2008, **2**, 257–259.
36 Z. Chem, M. G. Debije, T. Debaerdemaeker, P. Osswald and F. Würthner, *ChemPhysChem*, 2004, **5**, 137–140.
37 R. Kinderman, L. H. Slooff, A. R. Burgers, N. J. Bakker, A. Büchtemann, R. Danz and J. A. M. van Rosmalen, *J. Sol. Energy Eng.*, 2007, **129**, 277–282.
38 B. E. Hardin, E. T. Hoke, P. B. Armstrong, J.-H. Yum, P. Comte, T. Torres, J. M. J. Fréchet, M. K. Nazeeruddin, M. Grätzel and M. D. McGehee, *Nat. Photonics*, 2009, **3**, 406–411.
39 G. Seybold and G. Wagenblast, *Dyes Pigm.*, 1989, **11**(4), 303–317.
40 B. Pagoaga, L. Giraudet and N. Hoffmann, *Eur. J. Org. Chem.*, 2014, 5178–5195.
41 Y. H. Cai, L. J. Huo, X. B. Sun, D. H. Wei, M. S. Tang and Y. M. Sun, *Adv. Energy Mater.*, 2015, **5**, 1500032.
42 Y. H. Cai, X. Y. Guo, X. B. Sun, D. H. Wei, M. M. Yu, L. J. Huo and Y. M. Sun, *Sci. China Mater.*, 2016, **59**, 427–434.
43 B. A. R. Günther, S. Höfener, R. Eichelmann, U. Zschieschang, H. Wadepohl, H. Klauk and L. H. Gade, *Org. Lett.*, 2020, **22**, 2298–2302.
44 L. Ji, M. Haehnel, I. Krummenacher, P. Biegger, F. L. Geyer, O. Tverskoy, M. Schaffroth, J. Han, A. Dreuw, T. B. Marder and U. H. F. Bunz, *Angew. Chem., Int. Ed.*, 2016, **55**, 10498–10501.
45 P. Leowanawat, A. Nowak-Król and F. Würthner, *Org. Chem. Front.*, 2016, **3**, 537–544.
46 S. Kumar, J. Shukla, Y. Kumar and P. Mukhopadhyay, *Org. Chem. Front.*, 2018, **5**, 2254–2276.
47 M. Kozaki, K. Sugimura, H. Ohnishi and K. Okada, *Org. Lett.*, 2006, **8**, 5235–5238.
48 A. A. Haidry, J. Puskelova, T. Plecenik, P. Durina, J. Gregus, M. Truchly, T. Roch, M. Zahoran, M. Vargova, P. Kus, A. Plecenik and G. Plesch, *Appl. Surf. Sci.*, 2012, **259**, 270–275.
49 H. Fritzsche, *J. Non-Cryst. Solids*, 1971, **6**, 49–71.
50 K. Nagarajan, A. R. Mallia, V. S. Reddy and M. Hariharan, *J. Phys. Chem. C*, 2016, **120**, 8443–8450.
51 Z. Chen, U. Baumeister, C. Tschierske and F. Würthner, *Chem. – Eur. J.*, 2007, **13**, 450–465.
52 D. Gosztola, M. P. Niemczyk, W. Svec, A. S. Lukas and M. R. Wasielewski, *J. Phys. Chem. A*, 2000, **104**, 6545–6551.
53 M. Bixon, J. Jortner, J. Cortes, H. Heitele and M. E. Michel-Beyerle, *J. Phys. Chem.*, 1994, **98**, 7289–7299.
54 L. Chen, C. Li and K. Müllen, *J. Mater. Chem. C*, 2014, **2**, 1938–1956.
55 F. Nolde, J. Qu, C. Kohl, N. G. Pschirer, E. Reuther and K. Müllen, *Chem. – Eur. J.*, 2005, **11**, 3959–3967.
56 F. O. Holtrup, G. R. J. Müller, H. Quante, S. De Feyter, F. C. De Schryver and K. Müllen, *Chem. – Eur. J.*, 1997, **3**, 219–225.
57 R. Renner, B. Mahlmeister, O. Anhalt, M. Stolte and F. Würthner, *Chem. – Eur. J.*, 2021, DOI: 10.1002/chem.202101877.
58 S. Seifert, *Doctoral dissertation*, Julius-Maximilians-Universität Würzburg, 2017.
59 E. H. A. Beckers, S. C. J. Meskers, A. P. H. J. Schenning, Z. Chen, F. Würthner and R. A. J. Janssen, *J. Phys. Chem. A*, 2004, **108**, 6933–6937.
60 R. Englman and J. Jortner, *Mol. Phys.*, 1970, **18**, 145–164.
61 S. J. Stricker and R. A. Berg, *J. Chem. Phys.*, 1962, **37**, 814–822.
62 F. Würthner, *Chem. Commun.*, 2004, 1564–1579.
63 Z. Chen, U. Baumeister, C. Tschierske and F. Würthner, *Chem. – Eur. J.*, 2007, **15**, 450–465.
64 T. Lu and F. Chen, *J. Comput. Chem.*, 2012, **33**, 580–592.
65 R. Herges and D. Geuenich, *J. Phys. Chem. A*, 2001, **105**, 3214–3220.
66 D. Geuenich, K. Hess, F. Köhler and R. Herges, *Chem. Rev.*, 2005, **105**, 3758–3772.